Electronic Supplementary Information for:

Novel Iridium complexes with N-heterocyclic dicarbene ligands in light-driven water oxidation catalysis: photon management, ligand effect and catalyst evolution

Andrea Volpe,[a] Mirco Natali,[b] Claudia Graiff,[c] Andrea Sartorel,[a] Cristina Tubaro[a] and Marcella Bonchio[a]

[a] *Department of Chemical Sciences, University of Padova, via Marzolo 1, 35131 Padova, Italy.*
[b] *Department of Chemical and Pharmaceutical Sciences, University of Ferrara, via L. Borsari 46, 44121 Ferrara, Italy.*
[c] *Department of Chemistry, Life Sciences and Environmental Sustainability, University of Parma, Parco Area delle Scienze 17/A, 43124 Parma, Italy.*

Synthesis of the azolium salts and silver(I) complexes

Synthesis of 1,1'-dimethyl-3,3'-ethylene-5,5'-dibromo-bis(imidazolium) dibromide

A solution of 5-bromo-1-methyl-imidazole (0.64 g, 3.98 mmol) and 1,2-dibromoethane (0.38 g, 2.02 mmol) in 1,4-dioxane (20 mL) was heated to 100 °C for 24 hours. The mixture was then cooled to room temperature and filtered. The product (white solid) was washed with small portions of diethyl ether and dried under vacuum. Yield 73 %. ^{1}H NMR (d_6-dmso): δ = 3.78 (s, 6H, CH_3), 4.68 (s, 4H, CH_2), 7.98 (s, 2H, C*H*), 9.23 (s, 2H, NC*H*N).

General procedure for the synthesis of the Ag(I) complexes

The proper bis(azolium) salt (1 mmol) and Ag_2O (2.5 mmol) were placed in a round bottom flask. Under inert atmosphere, deionised water (50 mL) was added and the mixture was stirred for 24 hours under light exclusion. Subsequently, the reaction mixture was filtered through Celite and the filtrate was treated with NH_4PF_6 (2.1 mmol). The resulting precipitate was filtered off and dried under vacuum.

2Ag. White solid. ^{1}H NMR (d_6-dmso): δ = 3.77 (s, 12H, CH_3), 4.64 (s, 8H, CH_2), 7.63 (s, 4H, C*H*). ^{13}C NMR (d_6-dmso): δ = 38.1 (*C*H_3), 51.4 (*C*H_2), 106.5 (*C*Br), 123.0 (*C*H), carbene carbon not detected. ESI-MS$^+$ (CH_3CN): *m*/*z* 1057 $[Ag_2L_2PF_6]^+$. Anal. Calcd for $C_{20}H_{24}Ag_2Br_4F_{12}N_8P_2$: C, 20.07; H, 2.02; N, 9.37%. Found: C, 19.65; H, 1.59; N, 8.62%.

3Ag. White solid. ^{1}H NMR (d_6-dmso): δ = 3.93 (s, 12H, CH_3), 5.23 (s, 8H, CH_2), 7.31 (m, 4H, Ar-*H*), 7.42 (m, 4H, Ar-*H*), 7.57 (m, 4H, Ar-*H*), 7.69 (m, 4H, Ar-*H*). ^{13}C NMR (d_6-dmso): δ = 35.2 (*C*H_3), 47.1 (*C*H_2), 112.0 (Ar-*C*H), 113.1 (Ar-*C*H), 125.3 (Ar-*C*H), 135.0 (Ar-*C*), 188.4 (Ar-*C*), 191.0 (N*C*N). ESI-MS$^+$ (CH_3CN): *m*/*z* 940 $[Ag_2L_2PF_6]^+$, 398 $[Ag_2L_2]^{2+}$.

Table S1. Crystallographic data for complexes **2** and **3**.

Complex	**2**	**3**
Empirical formula	$C_{20}H_{27}Br_2ClF_6IrN_4P$	$C_{28}H_{33}ClF_6IrN_4P$
Formula weight	855.89	798.20
Temperature/K	293(2)	293(2)
Crystal system	monoclinic	monoclinic
Space group	$P2_1/n$	$P2_1/n$
a/Å	13.798(3)	14.439(3)
b/Å	12.135(2)	12.898(3)
c/Å	15.460(3)	15.652(3)
α/°	90	90
β/°	91.923(3)	92.895(3)
γ/°	90	90
Volume/$Å^3$	2587.2(8)	2911.2(11)
Z	4	4
$\rho_{calc}g/cm^3$	2.197	1.821
μ/mm^{-1}	8.476	4.798
F(000)	1632.0	1568.0
Crystal size/mm^3	0.18 × 0.17 × 0.15	0.20 × 0.18 × 0.17
Radiation	MoKα (λ = 0.71073)	MoKα (λ = 0.71073)
2Θ range for data collection/°	3.892 to 61.008	3.744 to 60.97
Index ranges	$-19 \le h \le 19$, $-17 \le k \le 17$, $-22 \le l \le 22$	$-20 \le h \le 20$, $-18 \le k \le 18$, $-22 \le l \le 22$
Reflections collected	41255	44448
Independent reflections	7868 [R_{int} = 0.0664, R_{sigma} = 0.0504]	8807 [R_{int} = 0.0443, R_{sigma} = 0.0375]
Data/restraints/parameters	7868/7/341	8807/0/377
Goodness-of-fit on F^2	0.982	1.012
Final R indexes [I>=2σ (I)]	R_1 = 0.0380, wR_2 = 0.0780	R_1 = 0.0276, wR_2 = 0.0518
Final R indexes [all data]	R_1 = 0.0672, wR_2 = 0.0905	R_1 = 0.0570, wR_2 = 0.0613
Largest diff. peak/hole / e $Å^{-3}$	1.45/-1.07	0.93/-0.72

$R_1 = \Sigma|Fo-Fc|/\Sigma(Fo)$; $wR_2 = [\Sigma[w(Fo^2-Fc^2)^2]/\Sigma[w(Fo^2)^2]]^{1/2}$.

Photogeneration of $Ru(bpy)_3^{3+}$

$Ru(bpy)_3^{2+} + h\nu \rightarrow {}^*Ru(bpy)_3^{2+}$

${}^*Ru(bpy)_3^{2+} + S_2O_8^{2-} \rightarrow Ru(bpy)_3^{3+} + SO_4^{2-} + SO_4^{\bullet-}$

$SO_4^{\bullet-} + Ru(bpy)_3^{2+} \rightarrow Ru(bpy)_3^{3+} + SO_4^{2-}$

Oxidation of Ir species

$Ru(bpy)_3^{3+}$ + **1a** $\rightarrow$ $Ru(bpy)_3^{2+}$ + **1a**$^+$ (primary hole scavenging likely involving oxidation of Ir(III) to Ir(IV)

further oxidation steps by $Ru(bpy)_3^{3+}$, leading to the formation of the catalyst resting state Ir(rest)

Water oxidation

4 $Ru(bpy)_3^{3+}$ + **Ir(rest)** $\rightarrow$ 4 $Ru(bpy)_3^{2+}$ + **Ir(act)**

Ir(act) + 2 H_2O $\rightarrow$ **Ir(rest)** + O_2 + 4 H^+

Scheme S1. Photocatalytic $Ru(bpy)_3^{2+}/S_2O_8^{2-}$ cycle, leading to activation of Ir species, and water oxidation catalysis. Photogeneration of the $Ru(bpy)_3^{3+}$ oxidant occurs by light absorption by the $Ru(bpy)_3^{2+}$ (λ_{max} = 450 nm, $\varepsilon = 1.4\times10^4$ $M^{-1}cm^{-1}$) and generation of a triplet excited state ${}^*Ru(bpy)_3^{2+}$; reaction of ${}^*Ru(bpy)_3^{2+}$ with $S_2O_8^{2-}$ follows (oxidative quenching of the photosensitizer) and generation of $Ru(bpy)_3^{3+}$ and of a sulfate radical anion $SO_4^{\bullet-}$; formation of a second equivalent of $Ru(bpy)_3^{3+}$ occurs by the reaction of the sulfate radical with $Ru(bpy)_3^{2+}$. Oxidation of Ir species starts from the initial complexes (**1a** is indicated for the sake of simplicity), and after several oxidation steps, involving also the organic ligand scaffold, leads to the catalyst resting state generally indicated as **Ir(rest)**. In the water oxidation, 4 oxidizing equivalents from $Ru(bpy)_3^{3+}$ are required to activate **Ir(rest)** to the active form **Ir(act)**, capable of generating oxygen, leading back to the formation of **Ir(rest)**.

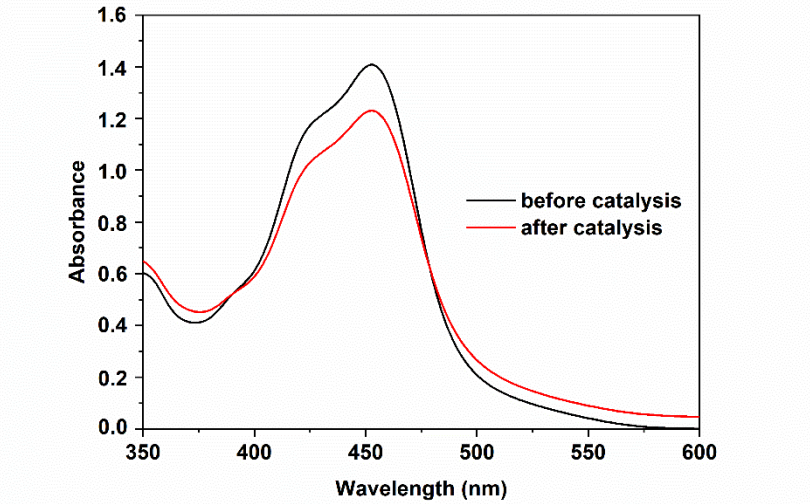

Figure S1. UV-Vis of reaction solution before and after light driven water oxidation. Conditions: Reaction conditions: 15 mL of 50 mM Na_2SiF_6/$NaHCO_3$ buffer, pH 5.2; $[Ru(bpy)_3^{2+}]$ = 1 mM; $[Na_2S_2O_8]$ = 5 mM; [**1a**] = 50 µM (loaded from a 2.5 mM solution in CH_3CN). Irradiation was performed with a series of six monochromatic LEDs emitting at 450 nm, with 1.06×10^{-7} einstein s^{-1} photon flux.

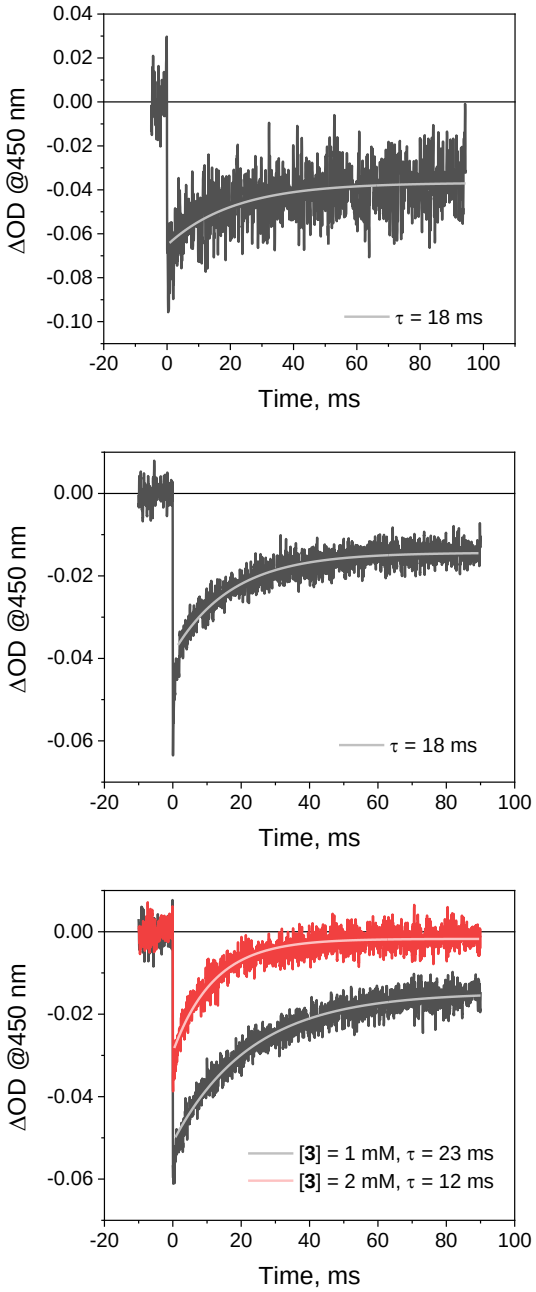

Figure S2. Kinetic traces at 450 nm obtained by laser flash photolysis (excitation at 355 nm) of 25/75 acetonitrile/10 mM Na_2SiF_6/$NaHCO_3$ buffer (pH 5.2) mixtures containing 50 μM $Ru(bpy)_3Cl_2 \cdot 6H_2O$, 50 mM $Na_2S_2O_8$, and 1 mM **1b** (top), 1 mM **2** (middle), and 1-2 mM **3** (bottom).

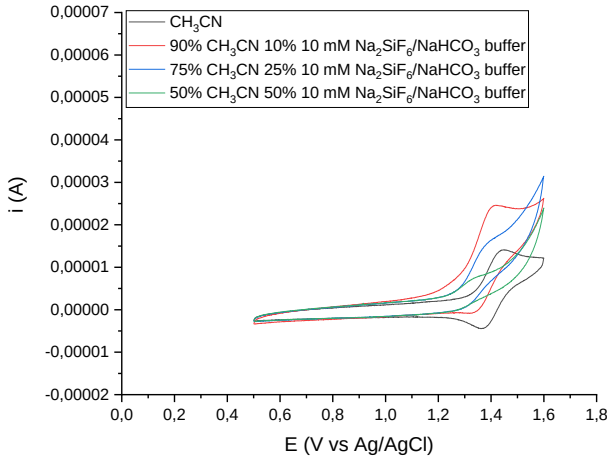

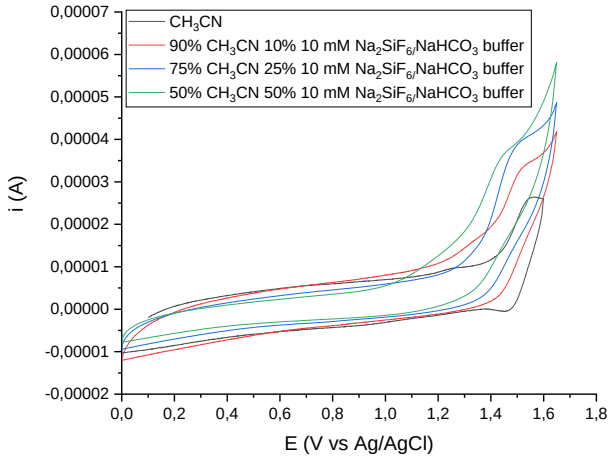

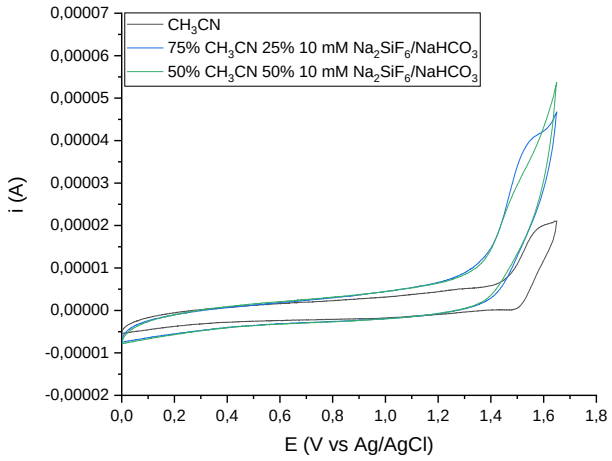

Figure S3. Cyclic voltammetries of 1a (top), 2 (middle) and 3 (bottom) in CH_3CN and in the presence of increasing amount of 10 mM aqueous $Na_2SiF_6/NaHCO_3$ buffer, pH 5.2. 0.1 M $(Et_4N)BF_4$ electrolyte, glassy carbon working electrode, platinum counter electrode, Ag/AgCl reference electrode, scan rate = 0.1 V s^{-1}.

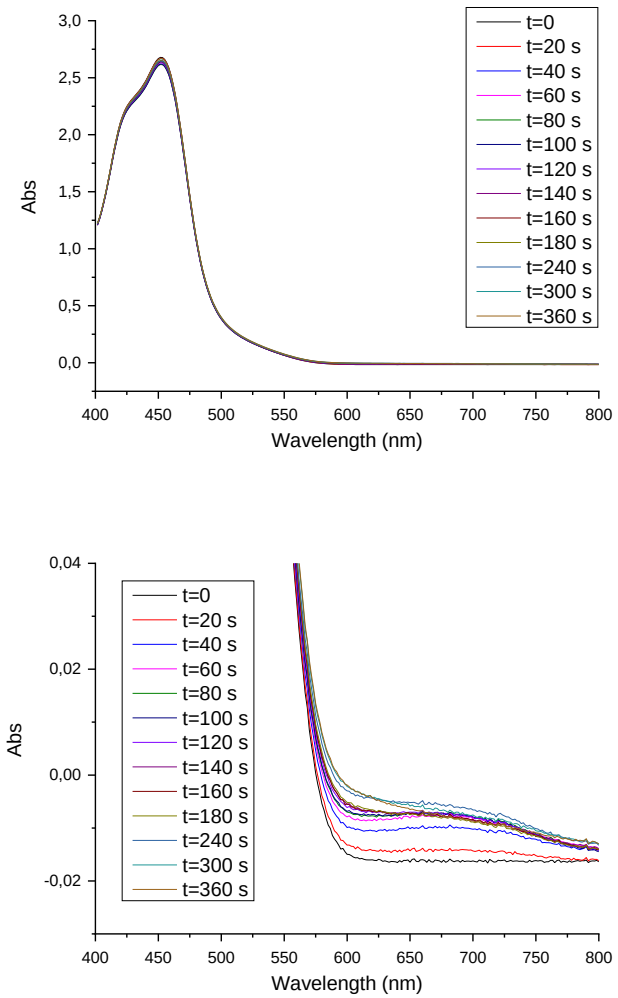

Figure S4. Absorbance spectra of a solution containing 200 µM **1a**, 1 mM $Ru(bpy)_3^{2+}$, 5 mM $S_2O_8^{2}$, in 50 mM Na_2SiF_6/$NaHCO_3$ buffer at different times upon illumination with white light (3.8 mW cm^{-2} at 20 cm distance) at 0-360 s irradiation The experiment was performed in a cuvette with 2 mm optical path.. Differential traces are reported in Figure 7 the main manuscript.

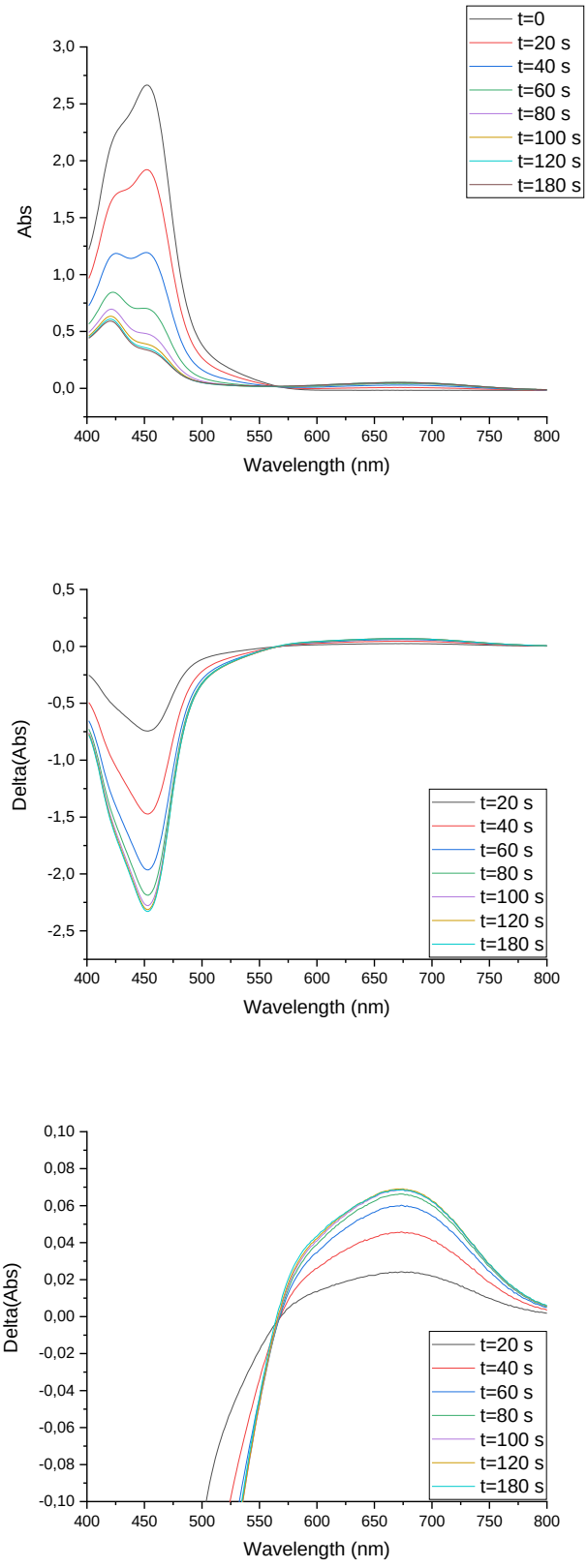

Figure S5. Top: absorbance spectra of a solution containing 1 mM $Ru(bpy)_3^{2+}$, 5 mM $S_2O_8^{2}$, in 50 mM $Na_2SiF_6/NaHCO_3$ buffer at different times upon illumination with white light (3.8 mW cm^{-2} at 20 cm distance) at 0-180 s irradiation The experiment was performed in a cuvette with 2 mm optical path. Middle and bottom: Differential traces.

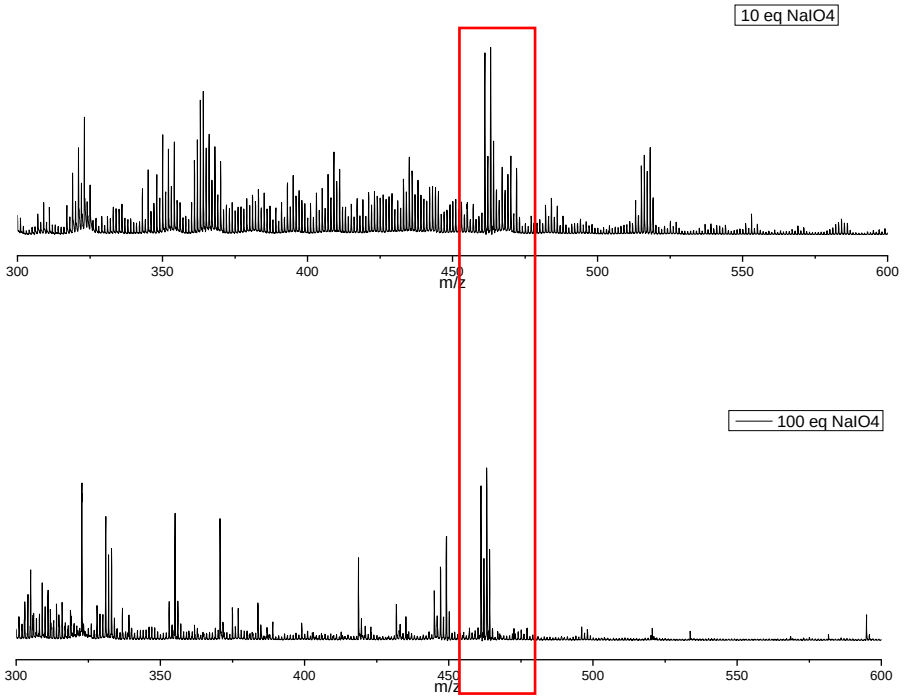

Figure S6. MALDI spectra of a solution of **1a** treated with 10-100 equivalents of $NaIO_4$.

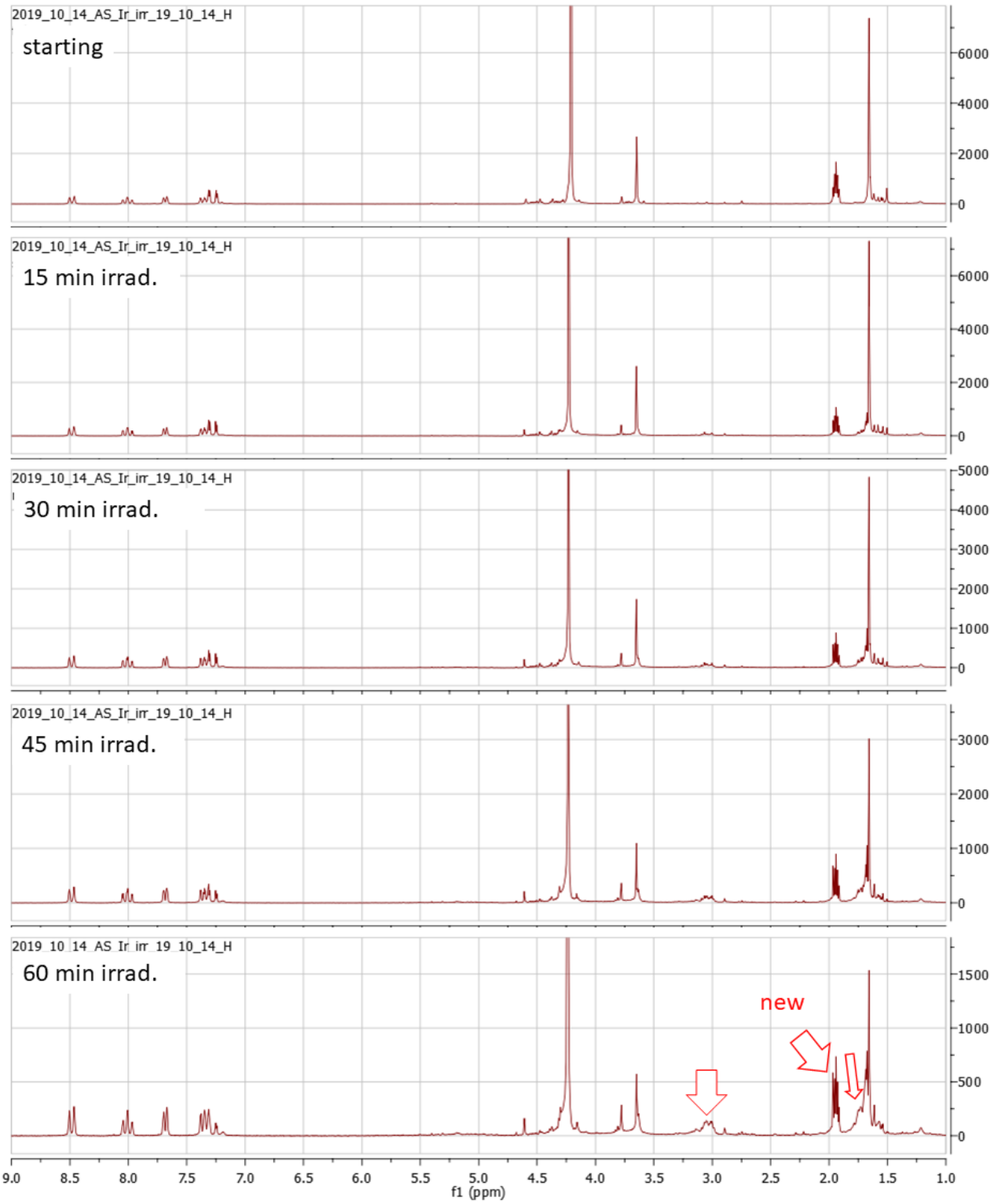

Figure S7. ^{1}H-NMR spectra of a 500 µl solution (50% CD_3CN / 50% 2.2 mM Na_2SiF_6+2.8 mM $NaHCO_3$ in D_2O), containing 5 mM **1a**, 1 mM $Ru(bpy)_3^{2+}$, 40 mM $Na_2S_2O_8$, under illumination with white light.

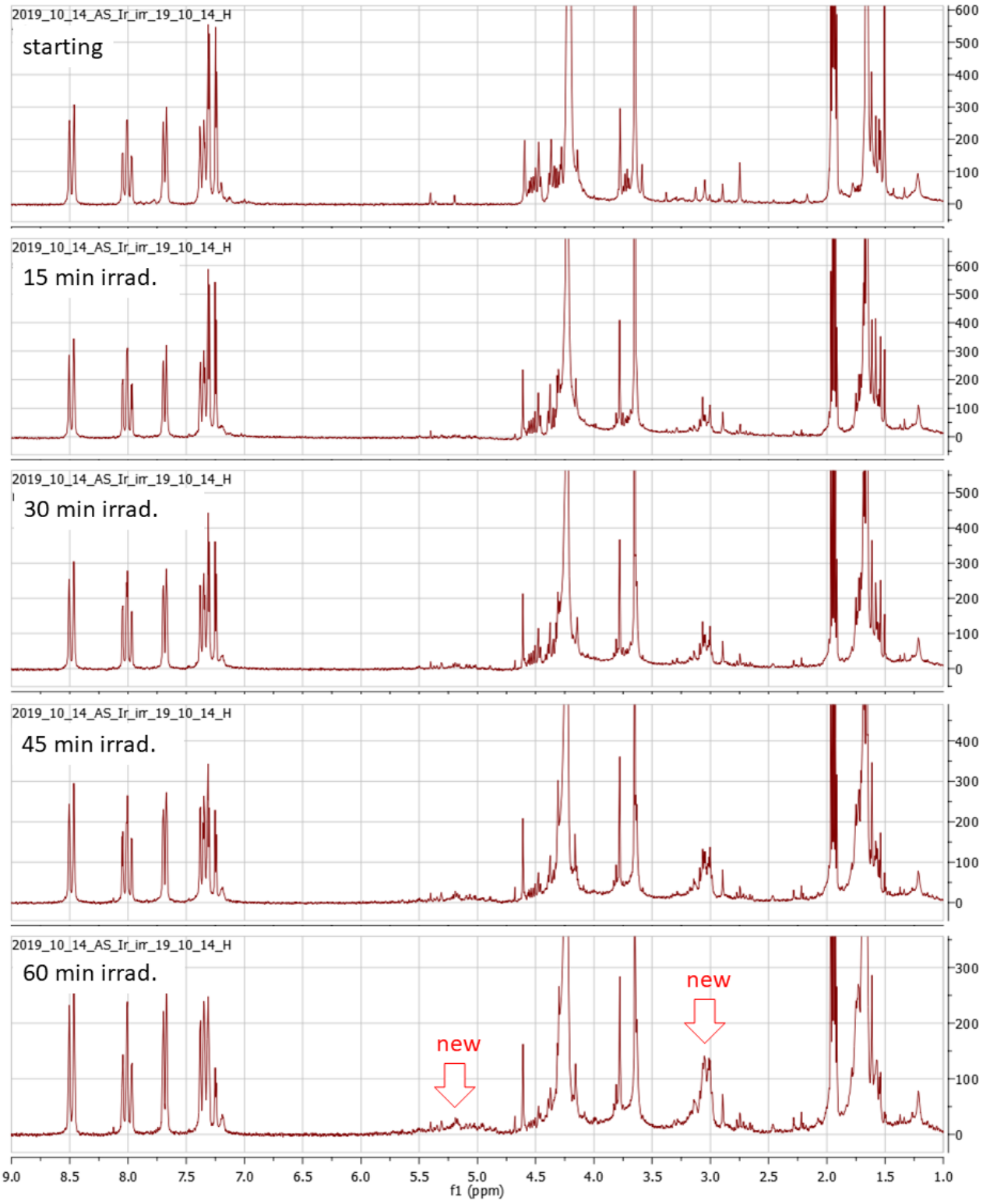

Figure S7 (continues). ^{1}H-NMR spectra of a 500 µl solution (50% CD_3CN / 50% 2.2 mM Na_2SiF_6+2.8 mM $NaHCO_3$ in D_2O), containing 5 mM **1a**, 1 mM $Ru(bpy)_3^{2+}$, 40 mM $Na_2S_2O_8$, under illumination with white light.

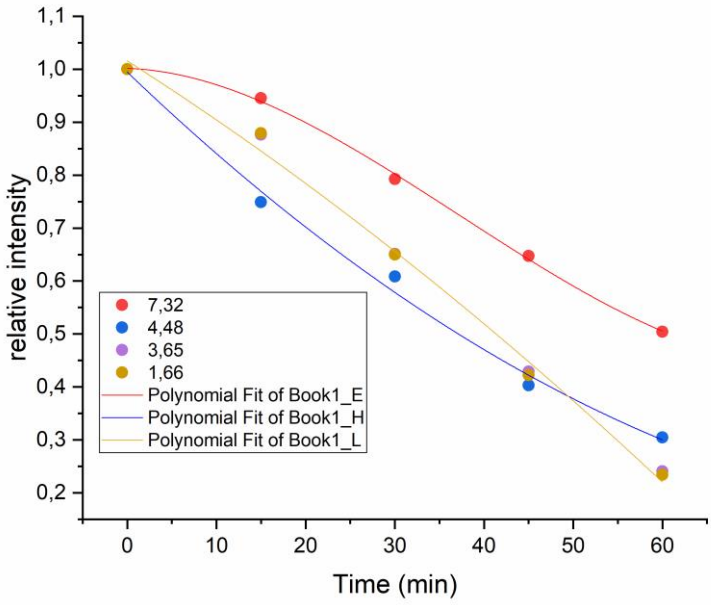

Figure S8. Height of the ^{1}H-NMR signals vs time along the irradiation of a 500 µl solution (50% CD_3CN / 50% 2.2 mM Na_2SiF_6+2.8 mM $NaHCO_3$ in D_2O), containing 5 mM **1a**, 1 mM $Ru(bpy)_3^{2+}$, 40 mM $Na_2S_2O_8$, under illumination with white light. The height was normalised with respect to the signal at 8.5 ppm and due to $Ru(bpy)_3^{2+}$. The height was used instead of the integration, given the complexity of the ^{1}H-NMR spectra and to the difficulty in integrating the signals. Attribution: signal at 7.32 ppm (red dots, C-H of the heterocyclic ring); signal at 4.48 ppm (blue dots, (N)-CH_2), signal at 3.65 ppm (purple dots, (N)-CH_3), 1.66 ppm (CH_3 of the Cp*).

NMR spectra of new compounds

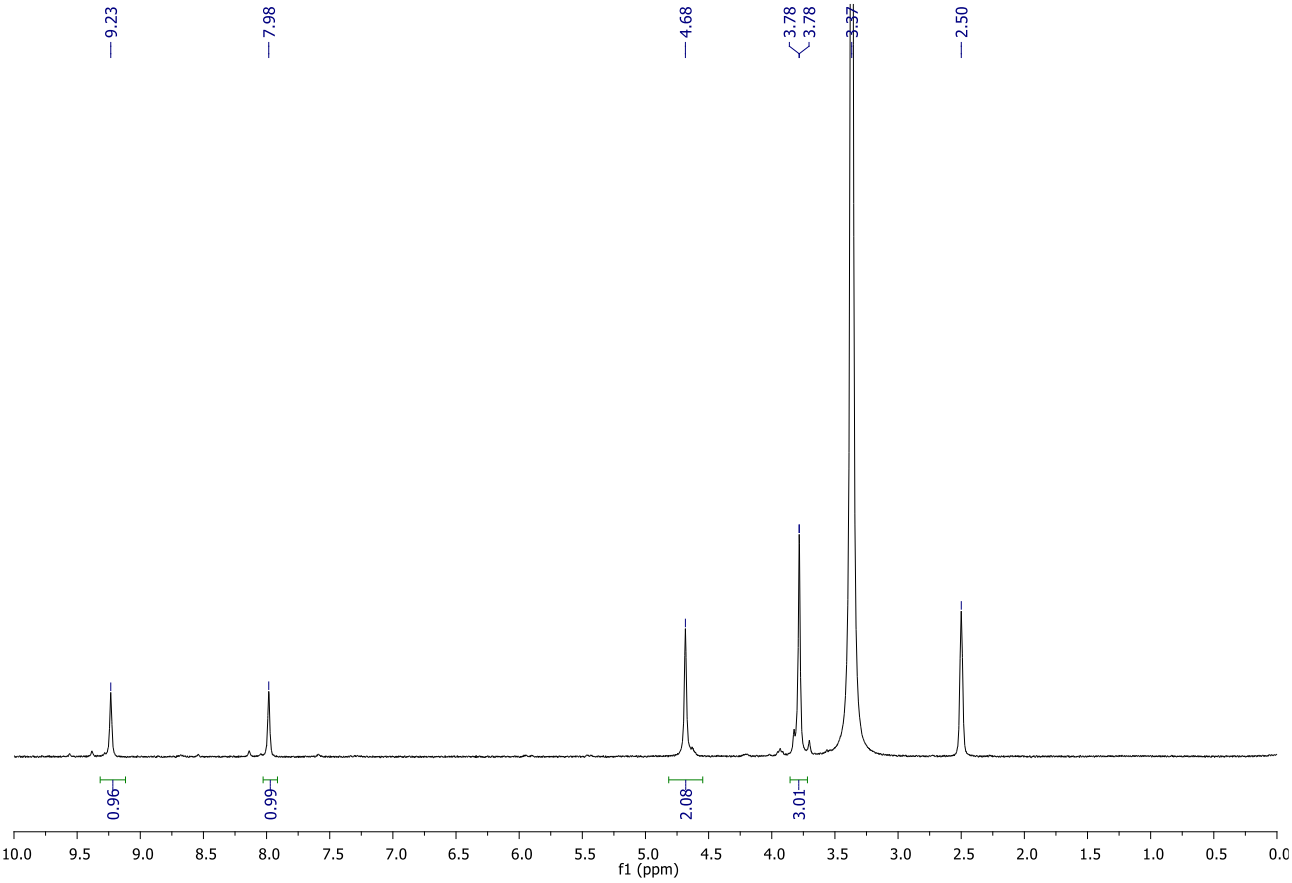

Figure S9. ^{1}H NMR spectrum of the diazolium salt 1,1′-dimethyl-3,3′-ethylene-5,5’-dibromo-bis(imidazolium) dibromide in DMSO-d_6.

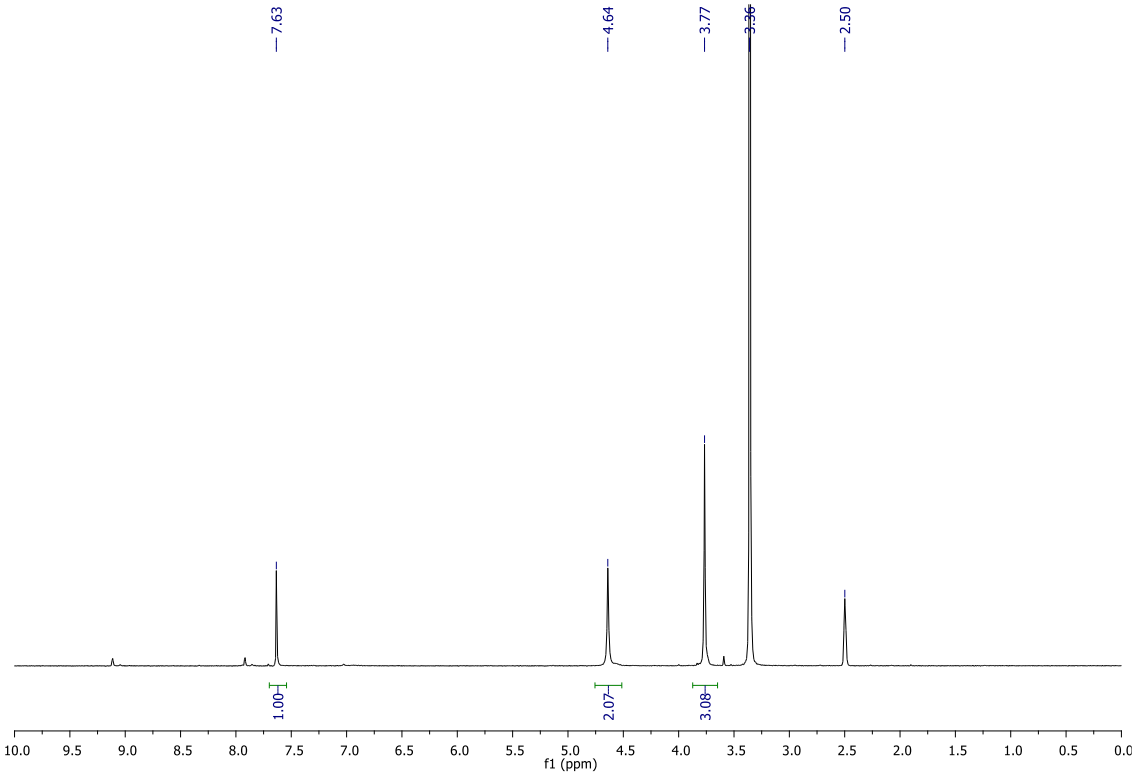

Figure S10. ^{1}H NMR spectrum of the silver complex **Ag2** in DMSO-d_6.

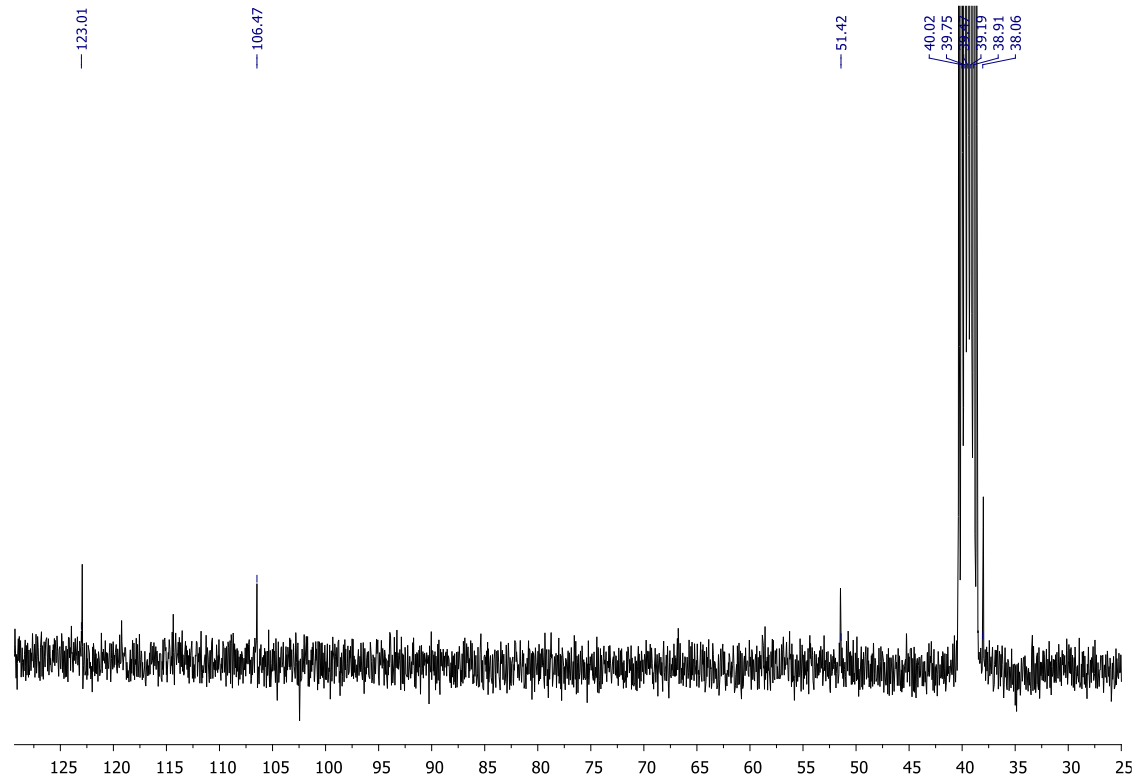

Figure S11. ^{13}C{^{1}H} NMR spectrum of complex **Ag2** in DMSO-d_6.

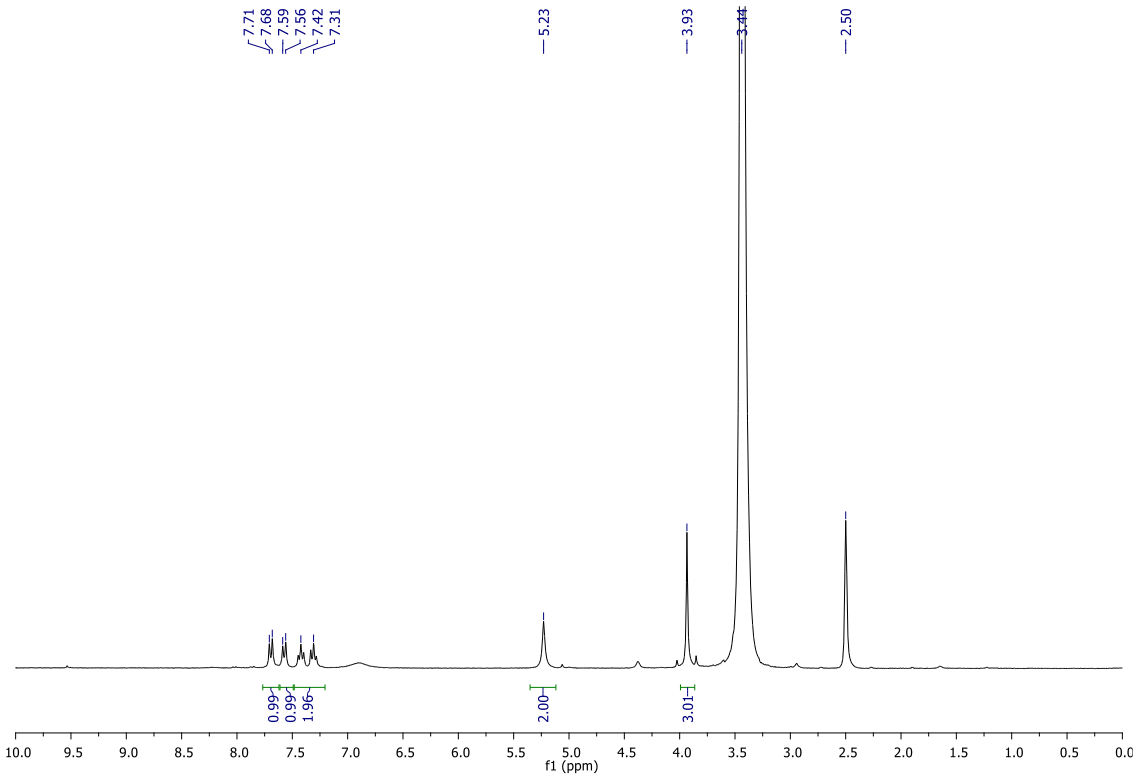

Figure S12. ^{1}H NMR spectrum of the silver complex **Ag3** in DMSO-d_6.

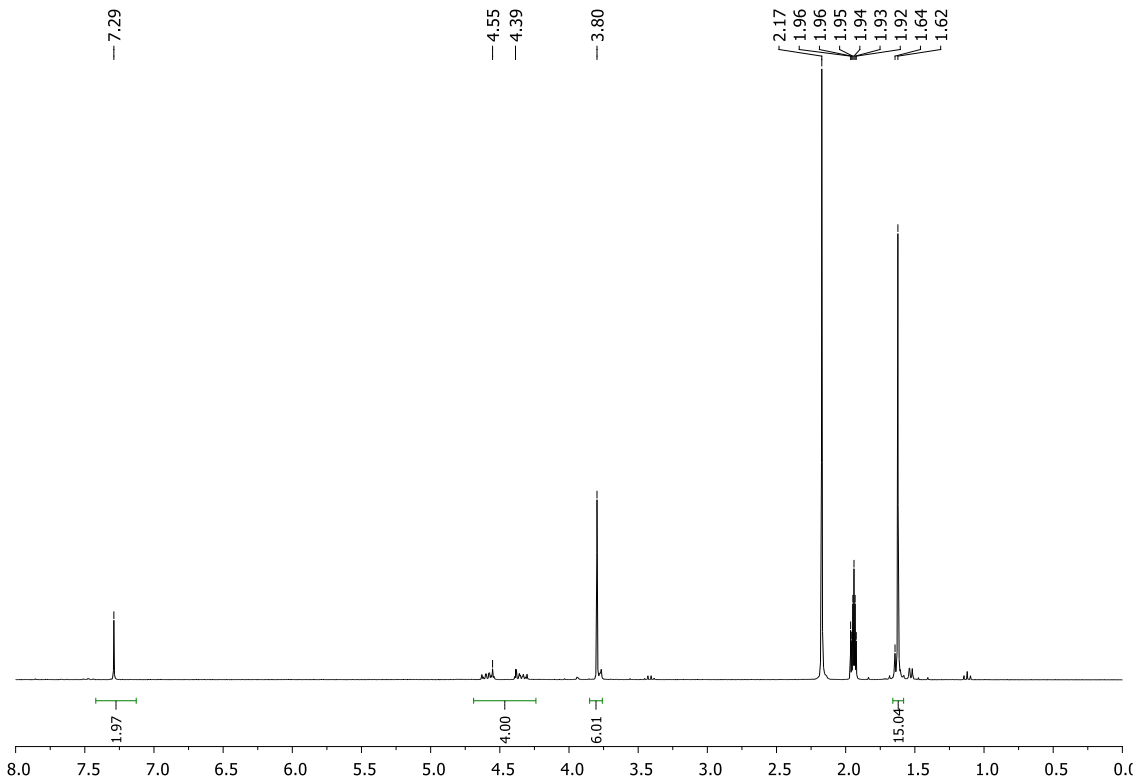

Figure S13. ^{1}H NMR spectrum of complex **2** in CD_3CN.

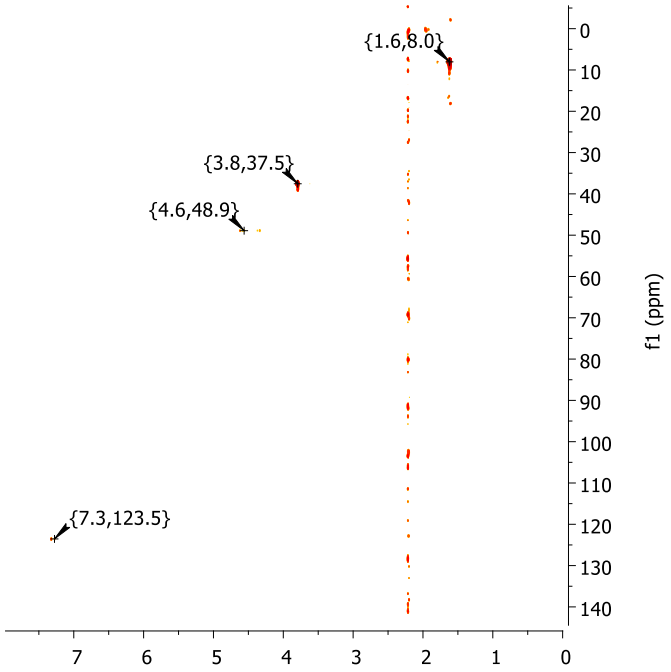

Figure S14. $^{13}C,^{1}H$ HMQC NMR spectrum of complex **2** in CD_3CN.

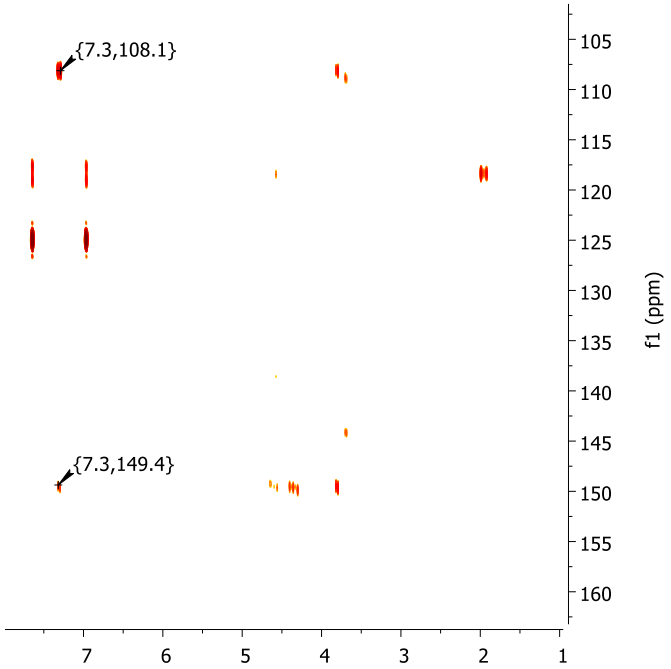

Figure S15. $^{13}C,^{1}H$ HMBC NMR spectrum of complex **2** in CD_3CN; detail on the CBr and carbene carbon cross-peaks.

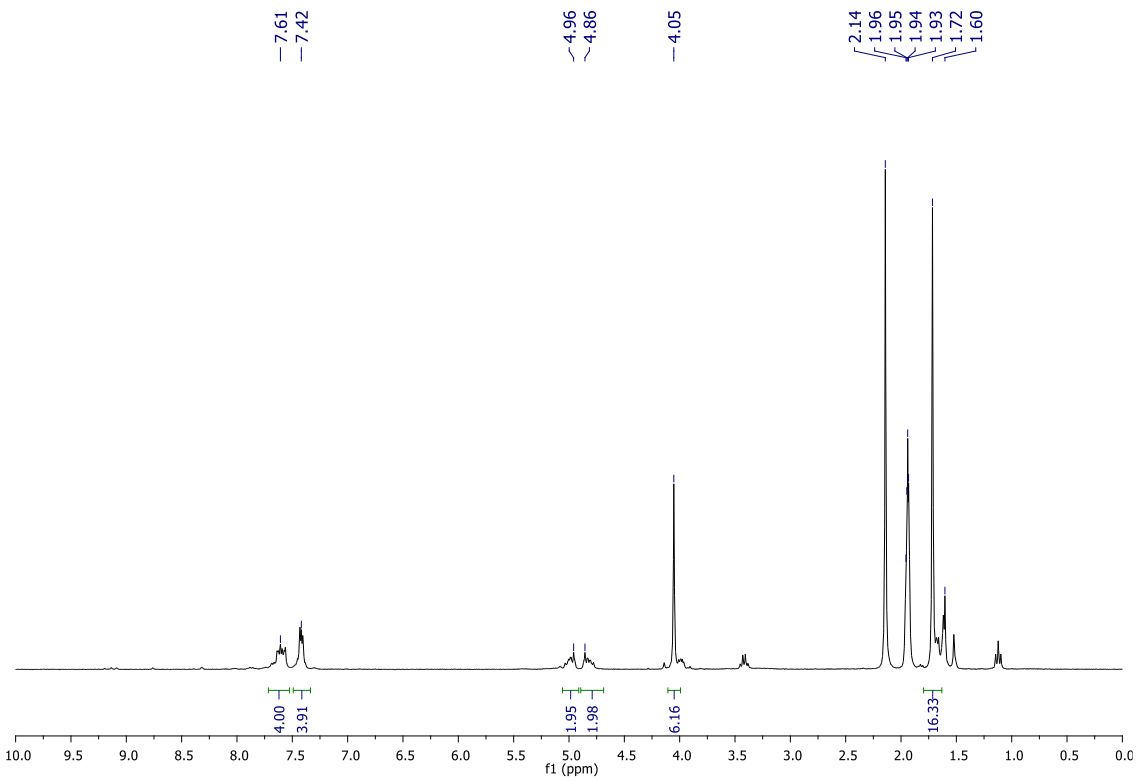

Figure S16. ^{1}H NMR spectrum of complex **3** in CD_3CN.

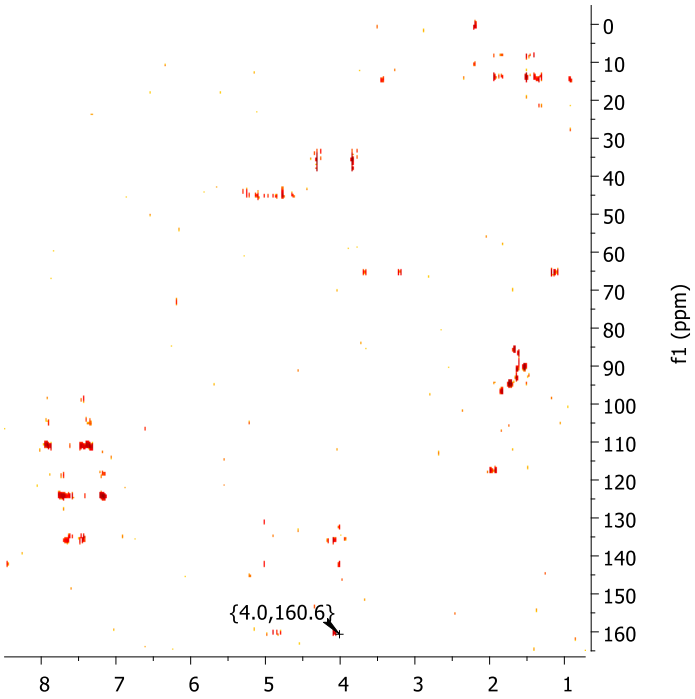

Figure S17. ^{13}C,^{1}H HMBC NMR spectrum of complex **3** in CD_3CN; detail on the carbene carbon cross-peaks.

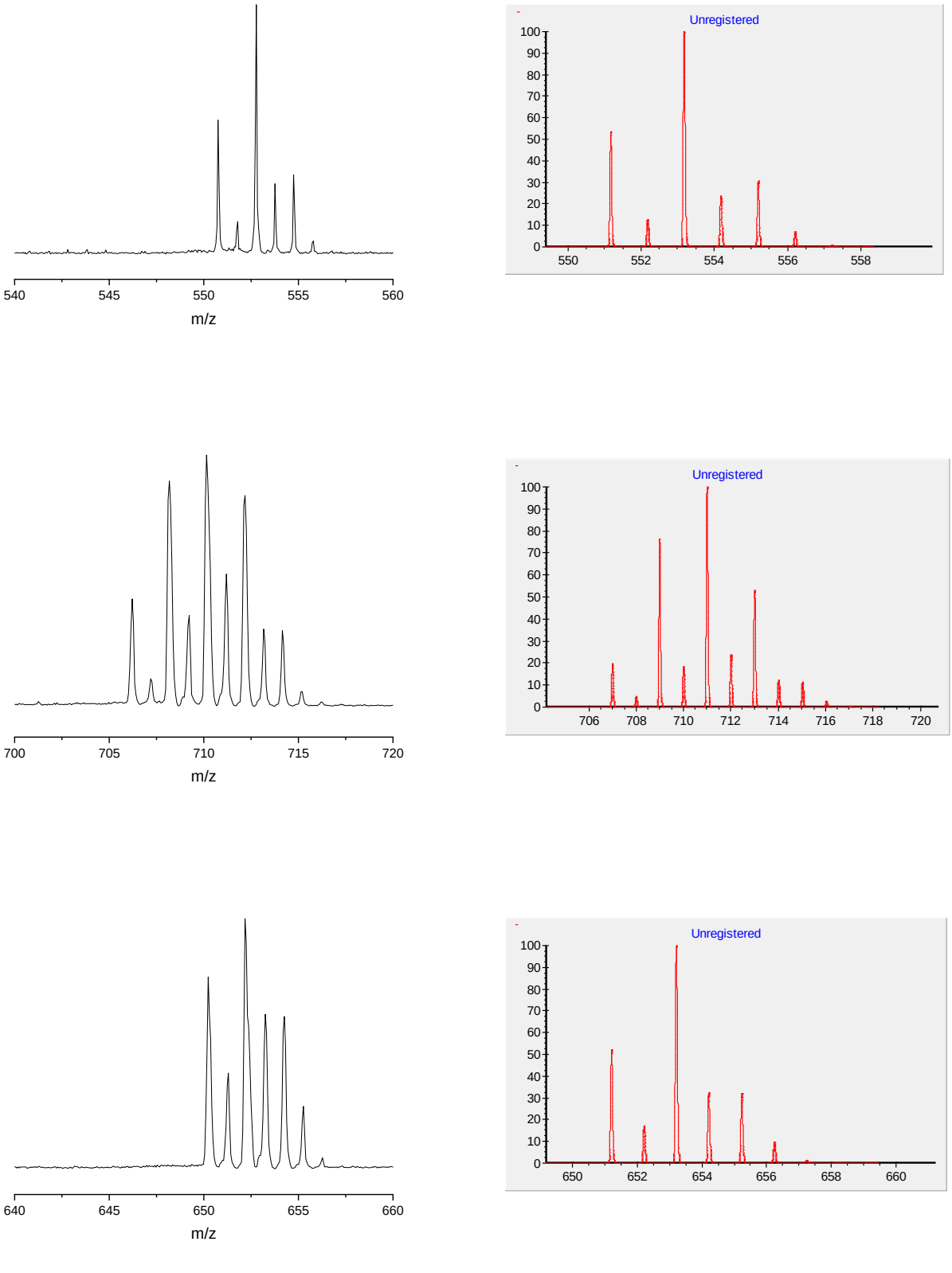

Figure S18. MALDI-MS signals of **1a** (top), **2** (middle) and **3** (bottom) with simulated isotopic patterns for the corresponding $[IrClCp^*diNHC]^+$ ions.